Computational Neuroscience Coursework

Sidney O'Neill

March 27, 2025

Question 1

(i, ii) Homogenous and Inhomogeneous Poisson Spike Trains

A homogeneous Poisson spike train was generated with a constant firing rate of 35 Hz, where inter-spike intervals (ISIs) were sampled from an exponential distribution. The model was extended to generate an inhomogeneous Poisson spike train, which had an absolute refractory period of $5ms$, ensuring no spikes could occur within this interval. The resulting spike trains were visualised with a raster plot, Figure 1a, and a histogram of ISIs, Figure 1b. All figures for this question were generated using a random seed of 1, unless otherwise stated.

$$\textbf{Homogeneous:} \quad \Delta t_i \sim \text{Exponential}\left(\frac{1}{r}\right), \quad t_{i+1} = t_i + \Delta t_i, \quad \text{for } t_i < T,$$

$$\textbf{Inhomogeneous:} \quad \Delta t_i \sim \text{Exponential}\left(\frac{1}{r}\right), \quad t_{i+1} = t_i + \Delta t_i, \quad \text{if } t_{i+1} - t_i \geq \Delta t_{\text{refr}},$$

where Δt_i is the ISI sampled from an exponential distribution with mean $1/r$ (where r is the firing rate in Hz), and $t_{i+1} = t_i + \Delta t_i$ continues for $t_i < T$, with Δt_{refr} introducing a refractory period.

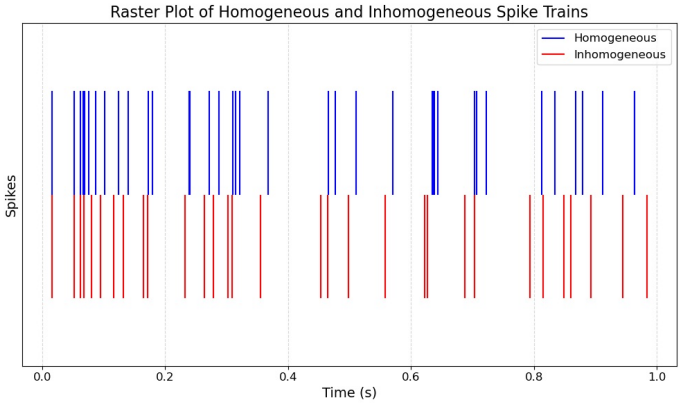

(a) The raster plot illustrates spike times for homogeneous (blue) and inhomogeneous (red) spike trains over $1s$, highlighting the constant firing rate of 35Hz for both trains and the refractory period of $5ms$ in the inhomogeneous train.

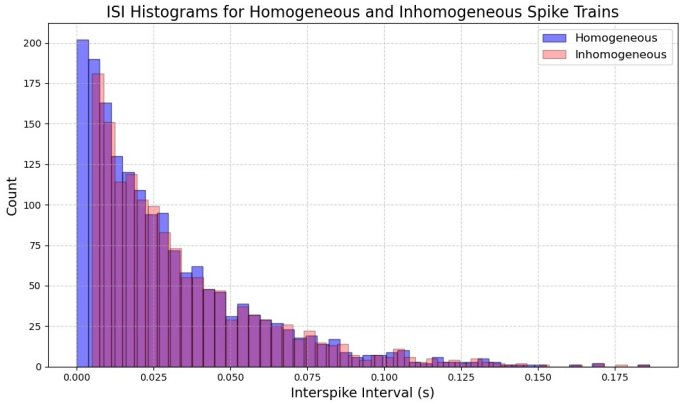

(b) The ISI histogram demonstrates the distribution of intervals between spikes, showing an exponential shape for both trains, with a noticeable rightward shift in the inhomogeneous train (due to $5ms$ refractory period). The duration was extended to $100s$ for better visualisation.

Figure 1: Comparison of spike train properties through raster plots and interspike interval (ISI) histograms.

The raster plot 1a shows that for the inhomogeneous spike trains, there are no instances where spikes occur within $5ms$ of each other, while the homogeneous spike trains show no such restriction. The ISI histogram 1b show that both spike trains have an exponential distribution of ISIs, while the inhomogeneous distribution is shifted $5ms$ to the right, reflecting the refractory period.

(iii, iv) Fano Factor and CV against window size and refractory period

The variability of the spike trains was analysed by calculating the spike-count Fano factor, which quantifies the variability in spike counts across time windows, and the ISI Coefficient of Variation (CV), a measure of the variability in interspike intervals. Table 1 shows the CV values, figure 2a against different window sizes and figure 2b shows CV and Fano factor against different refractory periods.

$$\textbf{Fano Factor:} \quad F = \frac{\sigma_k^2}{\mu_k},$$

$$\textbf{Coefficient of Variation (CV):} \quad C_v = \frac{\sigma_{\text{ISI}}}{\mu_{\text{ISI}}}.$$

where σ_k^2 is the variance of spike counts in time bins, and μ_k is the mean spike count, σ_{ISI} is the standard deviation of inter-spike intervals (ISI), and μ_{ISI} is their mean.

Process	CV (2 d.p.)
Homogeneous	0.99
Inhomogeneous	0.95

Table 1: CV values for Homogenous and Inhomogeneous processes (averaged over 100 runs)

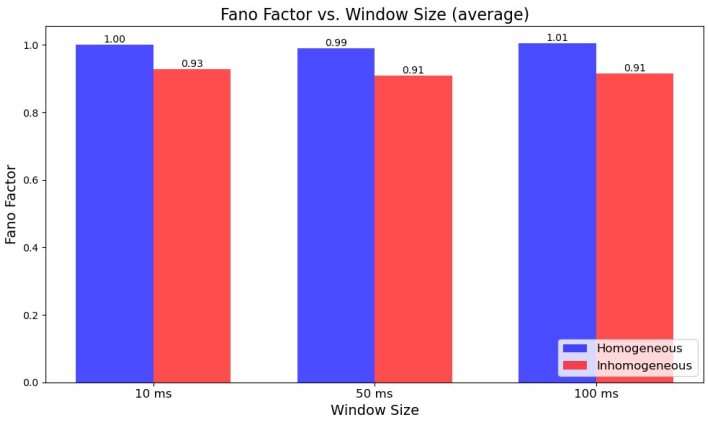

(a) The bar plot displays the Fano Factor of Homogeneous (blue) and Inhomogeneous (red) spike trains for different window sizes. Results were averaged over 100 runs.

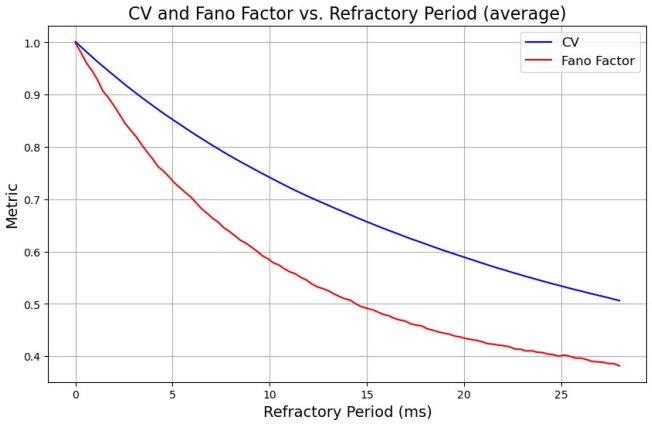

(b) The line plot depicts the variation of CV (blue) and Fano Factor (red) as functions of the refractory period in milliseconds. Results were averaged over 100 runs.

Figure 2: Analysis of spike train variability using Fano factor and ISI Coefficient of Variation (CV).

Figure 2a shows for the homogeneous process, the Fano Factor remains around 1, consistent with the fully random nature of a Poisson process. Small deviations can be attributed to statistical fluctuations and are not significant. In the inhomogeneous case, the introduction of a refractory period reduces randomness, as no spike can occur within this refractory period, leading to a lower Fano Factor Figure.

Figure 2b when the refractory period is $0ms$ the inhomogeneous process behaves as a homogeneous one, with Fano Factor and CV values at 1. As the refractory period increases, randomness is reduced, and both CV and Fano Factor decrease.

Question 2

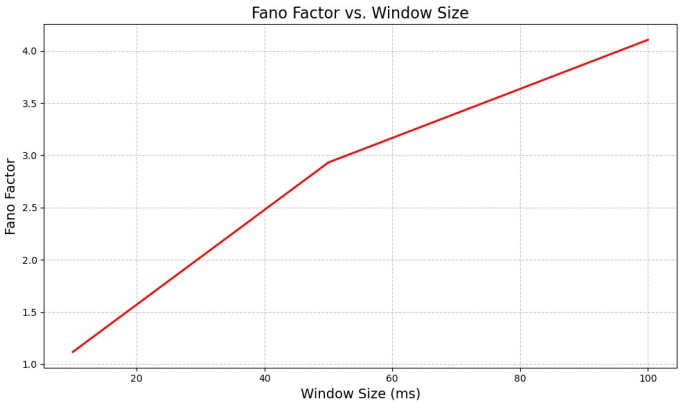

Figure 3: The line plot displays the Fano Factor as a function of window size (10 ms, 50 ms, and 100 ms) for the spike train in `rho.dat`, with the y-axis indicating Fano Factor values.

To evaluate the variability of the spike train, we first extracted spike times from the binary vector in `rho.dat` and we then computed the Fano Factor for window sizes of 10 ms, 50 ms, and 100 ms as well as the ISI CV.

Figure 3 and table 2 show the spike train in `rho.dat` exhibits greater variability than expected for a homogeneous Poisson process, as evidenced by a Fano factor that increases with window size, reaching approximately 4.0 for 100 ms bins (compared to the Poisson expectation of 1) and an ISI Coefficient of Variation (CV) of 2.01. This inhomogeneous Poisson-like behaviour may be attributed to the complex visual encoding required for processing dynamic visual stimuli in the fly's environment.

ISI Coefficient of Variation (CV)	2.01

Table 2: ISI Coefficient of Variation (CV) for the spike train in `rho.dat`.

Question 3

We modelled a leaky integrate-and-fire (LIF) neuron governed by the differential equation:

$$\tau_m \frac{dV}{dt} = E_L - V + R_m I_{\text{syn}}, \tag{1}$$

where V is the membrane potential, E_L is the leak potential, τ_m is the membrane time constant, R_m is the membrane resistance, and I_{syn} is the synaptic input current. The neuron fires when V exceeds a threshold and is reset to a lower potential. Synaptic input I_{syn} was modelled as a combination of excitatory and inhibitory Poisson inputs (I_{exc} and I_{inh}) scaled by synaptic strength (σ_{syn}), and with an underlying bias current (I_{bias}):

$$I_{\text{syn}} = \sigma_{\text{syn}} \cdot (I_{\text{exc}} - I_{\text{inh}}) + I_{\text{bias}}, \tag{2}$$

$$I_{\text{exc}} \sim \text{Poisson}\left(r_{\text{exc}} \cdot \frac{\Delta t}{1000}\right), \quad I_{\text{inh}} \sim \text{Poisson}\left(r_{\text{inh}} \cdot \frac{\Delta t}{1000}\right),$$

where r_{exc} and r_{inh} are the excitatory and inhibitory input rates, derived from a the total input rate r_{input} and the E/I ratio. We used Euler integration to simulate the neuron's voltage dynamics over time:

$$\Delta V = (E_L - V + R_m I_{\text{syn}}) \frac{\Delta t}{\tau_m}, \quad V \leftarrow V + \Delta V. \tag{3}$$

To maintain a constant post-synaptic firing rate (35 Hz), we iteratively adjusted the input rate. Figure 4 compares the voltage dynamics for adjusted and unadjusted input rates.

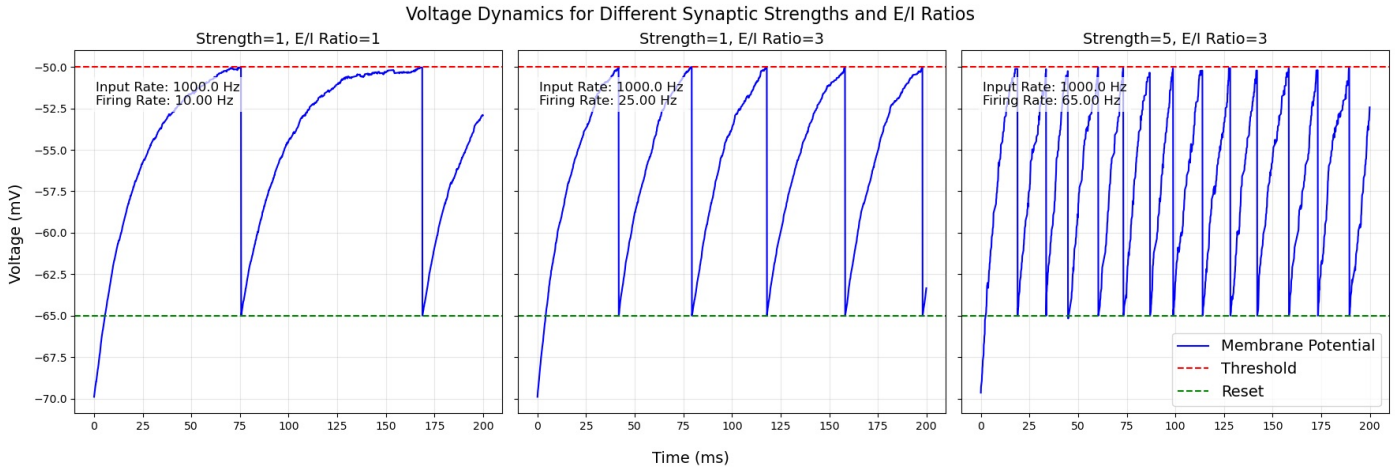

(a)

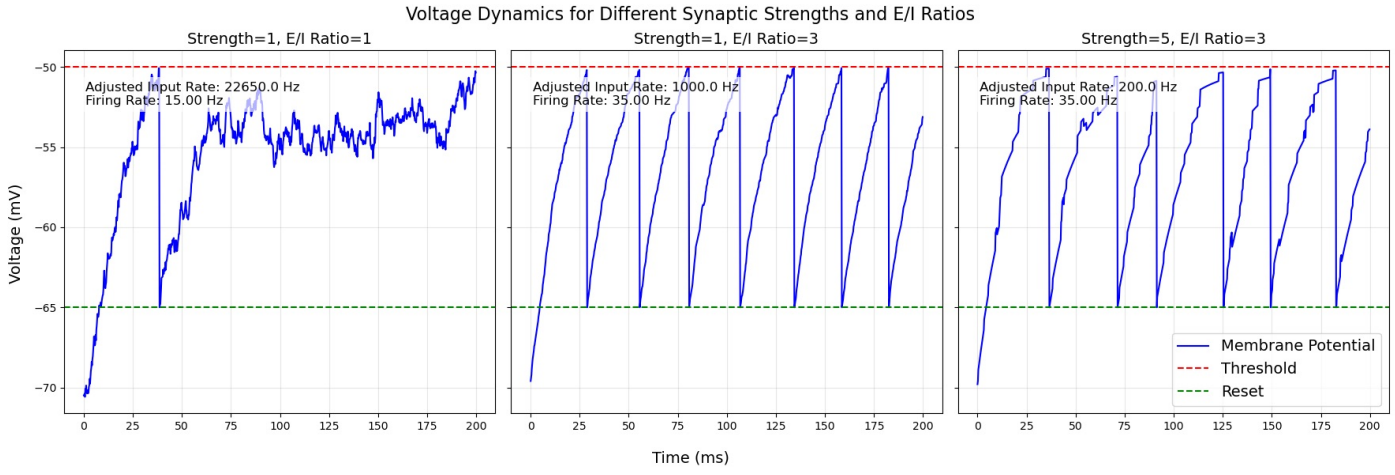

(b)

Figure 4: Voltage dynamic plots of the LIF model neuron simulated under varying synaptic strength and E/I ratio. The top row illustrates a constant input rate of 1000 Hz leading to different firing rates. The bottom row demonstrates adjusted input rates to achieve 35 HZ firing rate under the same synaptic conditions. The membrane potential (blue) reaches the threshold (red) to trigger a spike and then resets (green).

Figure 4b, illustrates the model successfully maintaining a 35 Hz firing rate. However, it also shows how a combination of low synaptic strength and low E/I ratio, as seen in the leftmost plot (strength = 1 and E/I ratio = 1), can be insufficient to consistently drive the voltage to the threshold, even with excessive input rates (22,650 Hz). However, this can be overcome by increasing I_{bias}. We then analysed how spike train variability changes with E/I input balance and synaptic strength, shown in 5.

In Figure 5a, the Fano Factor decreases logarithmically with increasing E/I ratio due to the stabilisation of spike variability as inhibitory inputs are overwhelmed by excitatory inputs. At low E/I ratios, inhibitory inputs dominate, leading to greater variability in interspike intervals and spike counts, reflected in a higher Fano Factor. However, as the E/I ratio increases, the variability decreases, and the neuron exhibits more regular firing patterns, leading to lower Fano Factor and CV values that converge toward a baseline.

Figure 5b shows how Fano Factor increases with synaptic strength due to the amplification of noise the input. Stronger synaptic currents amplify the variability inherent in Poisson-distributed inputs, leading to larger fluctuations in spike timing and counts. The CV also increases, albeit more gradually, reflecting greater irregularity in interspike intervals as synaptic strength grows. These trends highlight how increased synaptic strength introduces greater variability in the neuron's firing dynamics.

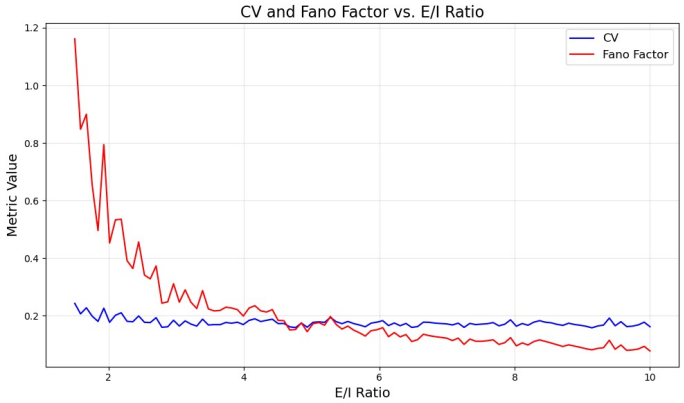

(a) CV (blue) and Fano Factor (red) as functions of the E/I ratio. The x-axis represents the (E/I) ratio, while the y-axis shows the metric values. The Fano Factor decreases logarithmically across the range of E/I ratios, while the CV remains relatively constant with slight fluctuations.

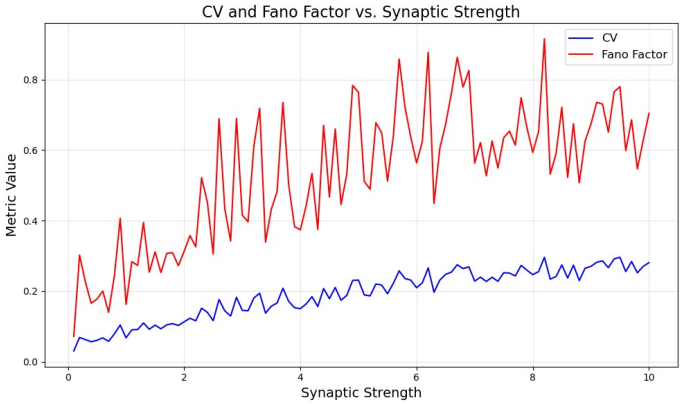

(b) CV (blue) and Fano Factor (red) as functions of synaptic strength. The x-axis represents synaptic strength, while the y-axis displays the metric values. The Fano Factor increases with noticeable fluctuations, while the CV exhibits an upward trend with less variability.

Figure 5: Comparison of CV and Fano Factor as functions of E/I ratio (a) and synaptic strength (b).

Question 4

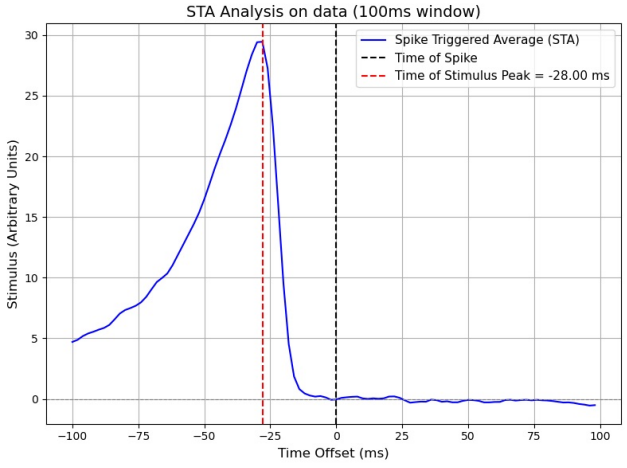

Figure 6: Spike-triggered average (STA) of `rho.dat` computed over a 100 ms window. The STA (blue) peaks at approximately -28 ms relative to the time of the spike (black).

To calculate the spike-triggered average (STA), the stimulus data (`stim.dat`) and spike train (`rho.dat`) were analysed. Spike times were extracted from the spike train, and for each spike, a 100 ms window of the preceding stimulus was averaged. The STA was computed by summing the stimulus segments aligned to each spike and dividing by the total number of spikes:

$$s(\tau) = \frac{1}{n} \sum_{i=1}^{n} x(t_i - \tau), \tag{4}$$

where $s(\tau)$ is computed as the average stimulus x preceding n spike times t_i, shifted by a lag τ. Figure 6 shows the spike-triggered average (STA), which represents the average stimulus pattern that precedes a spike. The x-axis indicates the time offset in milliseconds, with 0 ms corresponding to the spike time, and the y-axis shows the average stimulus intensity in arbitrary units. The peak at -28 ms suggests that a strong stimulus at this time offset is most likely to trigger a spike.

Question 5

We analysed the average stimulus preceding two spikes separated by specific intervals (2 ms, 4 ms, 10 ms, 20 ms, and 50 ms). The spike-triggered average (STA) was computed for two cases: adjacent spike pairs and non-adjacent spike pairs. For each interval, the stimulus segments were aligned relative to the second spike in the pair, averaged, and compared between the two scenarios.

Figure 7a shows all the STA profiles of non-adjacent and adjacent pairs. There are no differences between the STA profiles for adjacent and non-adjacent pairs within the short intervals (2 ms and 4 ms). The lack of difference between the 2 ms and 4 ms groups can most likely be attributed to the refractory period being greater than 4 ms. This ensures that only adjacent spike pairs can occur within this interval, as the refractory period prevents a second spike from happening in such a short time frame. At longer intervals (10 ms, 20 ms, and 50 ms), distinct differences emerge.

As shown in Figure 7b shows more clearly, adjacent spikes exhibit a characteristic dip that follows these peaks, which likely occurs because of the neuron's refractory period, which suppresses firing shortly after the first spike. The dip represents the reduced likelihood of spiking due to the refractory constraint. In contrast, non-adjacent spike pairs occur over longer intervals, allowing sufficient recovery time from the refractory period, leading to broader STA profiles.

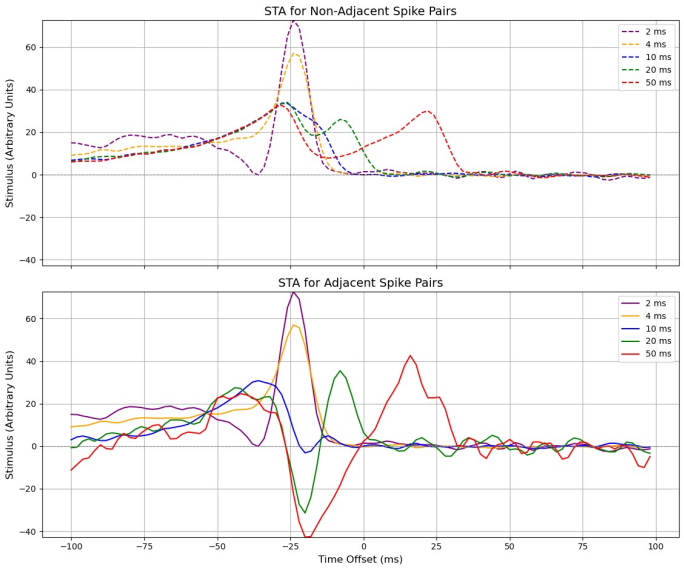

(a) The spike-triggered average (STA) for non-adjacent spike pairs (top) and adjacent spike pairs (bottom) across different interspike intervals (2 ms, 4 ms, 10 ms, 20 ms, and 50 ms). The STA for non-adjacent pairs shows broader peaks with no pronounced dips, while the STA for adjacent pairs exhibits sharper peaks and dips after the peak.

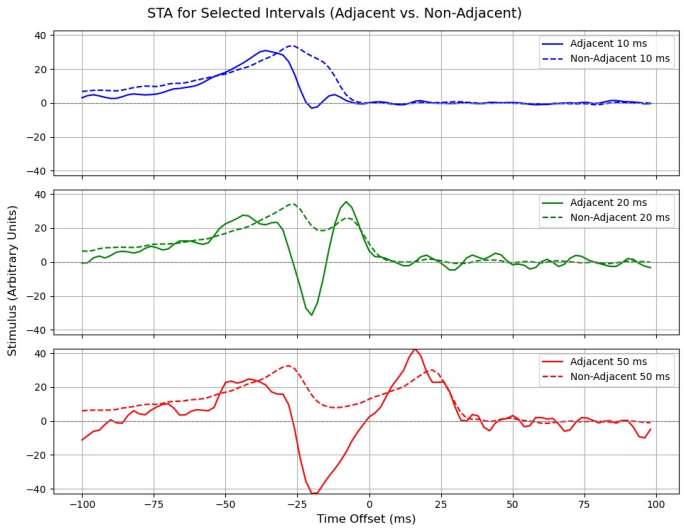

(b) The spike-triggered average (STA) for adjacent (solid lines) and non-adjacent (dashed lines) spike pairs at selected longerintervals (10 ms, 20 ms, and 50 ms). Adjacent spike pairs display sharper peaks and distinct dips following the peak due to the refractory period, while non-adjacent pairs show broader, smoother STAs.

Figure 7: Comparison of STA plots for adjacent and non-adjacent spike pairs at different intervals.

Question 6

The stimulus data from the `stim.dat` file was used as input to the leaky integrate-and-fire (LIF) neuron model described in Equation 1. The synaptic input current seen in Equation 2 was modified as follows:

$$I_e = \sigma_{\text{syn}} \cdot \texttt{stim}[t_{\text{idx}}] + I_{\text{bias}},$$

where $\texttt{stim}[t_{\text{idx}}]$ corresponds to the stimulus value at the current time step. Using the spike times generated by the LIF model from this stimulus data, we computed the STA using Equation 4. This approach enabled a direct comparison of the simulated STA with the actual STA derived from the spike train provided in the `rho.dat` file.

To investigate the effects of varying synaptic strength and the membrane time constant (τ_m), these parameters were systematically adjusted. We experimented with σ_{syn} between 1 and 10, while τ_m was varied between 30 ms and 5 ms. The resulting simulated STA profiles for different variations in strength and τ are shown in Figure 8, indicating how increasing strength and decreasing τ_m both lead to a smoother STA profile.

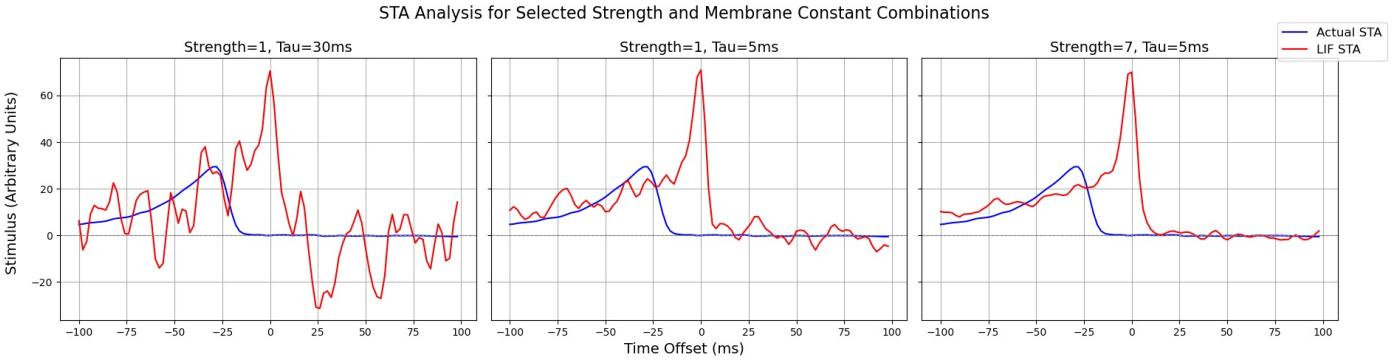

Figure 8: STA analysis comparing actual STA (blue) and LIF model STA (red) for different combinations of synaptic strength and membrane time constant (τ)

However, there were still some key differences between the simulated STA and the actual STA. Firstly, there was a much sharper peak observed in the simulated LIF STA. The experimental data inherently incorporates the noise present in biological systems while LIF model does not leading to exaggerated, tightly synchronised responses to the input stimulus. Plot 2 of Figure 9 displays how increasing the simulation's time step to 5 ms better approximated the inherent temporal filtering by smoothing the simulated STA peak.

In the `rho.dat`, the neuronal responses measured include contributions from numerous sources of noise. These stochastic processes reduce the precision and sharpness of spike timing relative to the stimulus. In contrast, the LIF model without noise lacks this biological variability, resulting in unrealistically precise spikes. This precision enhances the STA peak because spikes are consistently timed with the most prominent features of the stimulus, leading to artificially high values in the STA. We incorporated noise into the Euler method seen in Equation 3 as follows:

$$dV = ((E_L - V) + R_m \cdot I_e) \cdot \left(\frac{\Delta t}{\tau_m}\right) + \mathcal{N}(0, \sigma_{\text{noise}})$$

where, $\mathcal{N}(0, \sigma_{\text{noise}})$ represents Gaussian noise with a mean of 0 and a standard deviation of σ_{noise}. Plot 3 of Figure 9 shows how the addition of noise with std=10 smooths the STA and decreases its peak value.

A further assumption of the LIF model is that it assumes an immediate response to the input stimulus, neglecting any delay in synaptic transmission. In biological systems, such as the fly H1 neuron that the `rho.dat` data represents, synaptic transmission is not instantaneous. Delays occur due to biological constraints, resulting in a temporal lag between the stimulus and the neuronal response. This delay is reflected in the shifted peak of the actual STA to -28 ms. To take account of this we introduced a synaptic delay term (Δt_{syn}) to the LIF model:

$$I_{\text{e}}(t) = \sigma_{\text{syn}} \cdot \texttt{stim}[t - \Delta t_{\text{syn}}] + I_{\text{bias}},$$

where Δt_{syn} shifts the stimulus input to mimic the temporal dynamics of real synaptic processing. Adding a delay of $\Delta t_{\text{syn}} = 28$ ms shifted it closer to the actual data, as shown in the final plot of Figure 9.

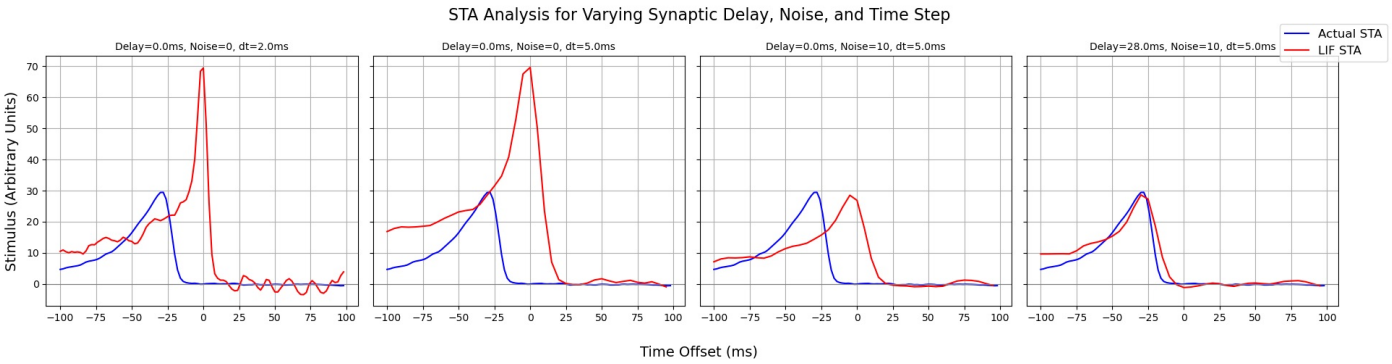

Figure 9: STA analysis comparing actual STA (blue) and LIF model STA (red) under varying synaptic delay, noise, and time step conditions: (left) delay = 0 ms, noise = 0, $\Delta t = 2$ ms; (center-left) delay = 0 ms, noise = 0, $\Delta t = 5$ ms; (center-right) delay = 0 ms, noise = 10, $\Delta t = 5$ ms; (right) delay = 28 ms, noise = 10, $\Delta t = 5$ ms. The parameter values the generated the final plot that closest matched the actual STA can be seen in Table 4.

We extended the analysis to include spike pairs, comparing the STA for both adjacent and non-adjacent spike pairs. Figure 10 shows the STA profiles for adjacent and non-adjacent spike pairs for both the actual `rho.dat` spike trains and simulated spike trains. To produce STA profiles for spike pairs from the LIF model that closely matched those derived from the actual data, we manually experimented with the parameters of the LIF model. These parameters included the synaptic strength, membrane time constant (τ_m), and bias current. Table 5 in the Appendix summarises the parameter values that resulted in the closest match between the actual and simulated STA profiles for spike pairs.

Once again, a consistent shift of the simulated STA peaks to align closely at 0 ms can be observed. It also further emphasises how STA peaks in the simulated LIF model are noticeably higher. Despite some limitations, with some experimentation with the parameter tuning and definition of the LIF model, we were able to show meaningful similarity. This indicates that the LIF model, while simplified, can capture important aspects of neuronal dynamics observed in the data. Furthermore, by tuning its parameters, the LIF model can provide valuable insights into neuronal behaviour, helping to explore how real neurons process inputs and respond under different conditions.

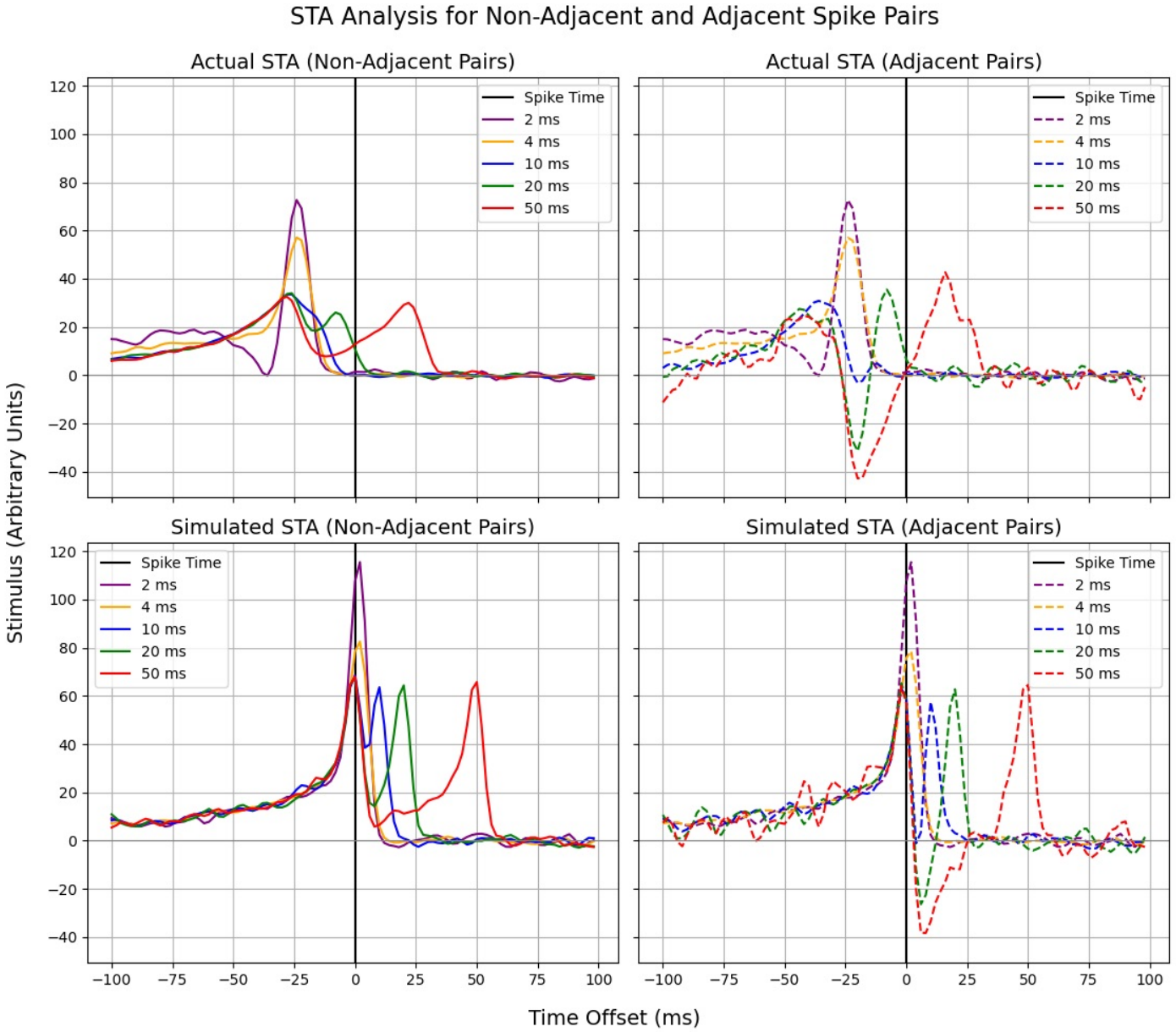

Figure 10: STA analysis for non-adjacent and adjacent spike pairs, comparing actual and simulated data. The figure presents the STA for non-adjacent spike pairs (left column) and adjacent spike pairs (right column) for both actual spike-triggered data, originally shown in Figure 7 (top row) and simulated data using a LIF neuron model (bottom row). The STA curves are shown for intervals of 2 ms, 4 ms, 10 ms, 20 ms, and 50 ms. The black vertical line marks the spike time (0 ms). The x-axis shows the time offset from the spike event in milliseconds, spanning 100 ms before and after the spike. The y-axis represents the stimulus in arbitrary units. The parameter values used to generate the results can be seen in Table 5.

A Appendix

Parameter	Symbol/Value	Description
Leak potential	$E_L = -70.0\,\text{mV}$	Resting membrane potential
Reset potential	$V_{\text{reset}} = -65.0\,\text{mV}$	Potential after a spike
Spike threshold	$V_{\text{threshold}} = -50.0\,\text{mV}$	Voltage at which the neuron spikes
Membrane time constant	$\tau_m = 20.0\,\text{ms}$	Time constant of the membrane
Membrane resistance	$R_m = 10.0\,\text{M}\Omega$	Membrane resistance
Time step	$\Delta t = 0.2\,\text{ms}$	Simulation time step
Simulation time for Fig 4	$T = 200.0\,\text{ms}$	Total simulation duration
Simulation time for Fig 5	$T = 1000.0\,\text{ms}$	Total simulation duration
Bias current	$I_{\text{bias}} = 2.0\,\text{nA}$	Constant depolarizing current
Input rate	$r_{\text{input}} = 1000.0\,\text{Hz}$	Initial synaptic input rate
Target firing rate	$r_{\text{target}} = 35.0\,\text{Hz}$	Desired post-synaptic firing rate
Firing rate tolerance	$\pm 0.5\,\text{Hz}$	Allowable deviation from the target
Synaptic strength range	$\sigma_{syn} = [0.2, 10]$	Range of values used
E/I ratio range	$E/I = [0.1, 10]$	Range of values used

Table 3: Outlines the constants and parameters used for the leaky integrate-and-fire (LIF) neuron simulation in Q3, including biophysical properties, simulation settings, and experimental conditions such as synaptic strengths and excitatory-to-inhibitory (E/I) ratios. When not being varied, $\sigma_{syn} = 7$ and E/I = 4. Values were used to generate Figure 4 and Figure 5

Parameter	Symbol/Value	Description
Leak potential	$E_L = -70.0\,\text{mV}$	Resting membrane potential
Reset potential	$V_{\text{reset}} = -65.0\,\text{mV}$	Potential after a spike
Spike threshold	$V_{\text{threshold}} = -50.0\,\text{mV}$	Voltage at which the neuron spikes
Membrane time constant	$\tau_m = 5.0\,\text{ms}$	Time constant of the membrane
Membrane resistance	$R_m = 10.0\,\text{M}\Omega$	Membrane resistance
Bias current	$I_{\text{bias}} = 2.0\,\text{nA}$	Constant depolarizing current
Time step (actual data)	$\Delta t_{\text{actual}} = 2\,\text{ms}$	Time step for actual data
Time step (simulation)	$\Delta t_{\text{simulation}} = 5\,\text{ms}$	Simulation time step values
Time window for STA	100 ms	Time window for Spike-Triggered Average
Synaptic strength	$\sigma_{syn} = 5.5$	Synaptic strength constant
Noise standard deviation	$std = 10$	Standard deviations for noise
Time Delay	$\Delta t_{syn} = 28\,\text{ms}$	Time delay added to LIF model

Table 4: Detailing the final parameter values used to generate the final result shown in Figure 9. These parameters were chosen to simulate the LIF neuron model accurately and calculate the Spike-Triggered Average.

Parameter	Symbol/Value	Description
Leak potential	$E_L = -70.0$ mV	Resting potential of the membrane
Reset potential	$V_{\text{reset}} = -65.0$ mV	Membrane potential after a spike
Spike threshold	$V_{\text{threshold}} = -50.0$ mV	Threshold for spike initiation
Membrane time constant	$\tau_m = 1.0$ ms	Time constant for membrane dynamics
Membrane resistance	$R_m = 10.0$ MΩ	Resistance of the membrane
Sampling interval	$\Delta t = 2$ ms	Time step used in simulation
Bias current	$I_{\text{bias}} = 2.0$ nA	Constant current driving the neuron
Synaptic strength	$\sigma_{\text{syn}} = 7.0$	Weight of the stimulus input
Time window	$t_{\text{window}} = 100$ ms	Window for STA calculation

Table 5: Detailing the parameter values used to generate the results shown in Figure 10. These parameters were utilized in the LIF neuron model and STA analysis to explore the effect of spike-pair intervals and time window on the computed results.